Diffusion processes in water on oxide surfaces: Quasielastic neutron scattering study of hydration water in rutile nanopowder

Xiang-qiang Chu,[1] Georg Ehlers,[1] Eugene Mamontov,[1,*] Andrey Podlesnyak,[1] Wei Wang,[2] and David J. Wesolowski[3]

[1]*Neutron Scattering Science Division, Oak Ridge National Laboratory, Oak Ridge, Tennessee 37831, USA*

[2]*Environmental Sciences Division, Oak Ridge National Laboratory, Oak Ridge, Tennessee 37831, USA*

[3]*Chemical Sciences Division, Oak Ridge National Laboratory, Oak Ridge, Tennessee 37831, USA*

(Received 22 June 2011; revised manuscript received 4 August 2011; published 30 September 2011)

Quasielastic neutron scattering (QENS) was used to investigate the diffusion dynamics of hydration water on the surface of rutile (TiO_2) nanopowder. The dynamics measurements utilizing two inelastic instruments, a backscattering spectrometer and a disk chopper spectrometer, probed the fast, intermediate, and slow motions of the water molecules on the time scale of picoseconds to more than a nanosecond. We employed a model-independent analysis of the data collected at each value of the scattering momentum transfer to investigate the temperature dependence of several diffusion components. All of the probed components were present in the studied temperature range of 230–320 K, providing, at a first sight, no evidence of discontinuity in the hydration water dynamics. However, a qualitative change in the elastic scattering between 240 and 250 K suggested a surface freezing-melting transition, when the motions that were localized at lower temperatures became delocalized at higher temperatures. On the basis of our previous molecular dynamics simulations of this system, we argue that interpretation of QENS data from such a complex interfacial system requires at least qualitative input from simulations, particularly when comparing results from spectrometers with very different energy resolutions and dynamic ranges.

DOI: 10.1103/PhysRevE.84.031505 PACS number(s): 61.20.Lc, 68.08.−p, 61.05.fg

I. INTRODUCTION

In recent years, significant progress has been made in understanding complex diffusion dynamics of surface water that readily hydrates hydrophilic surfaces, e.g., in oxides [1–10]. Under ambient conditions, such a hydration of TiO_2 (rutile) with the (110) crystal face predominant [8] results in three distinct structural layers of surface water, from the innermost L_1 to the intermediate L_2 to the outermost L_3, with L_1 including both intact water molecules and dissociated hydroxyl groups in direct contact with the crystalline surface [11]. The use of hydrated oxide nanopowders characterized by high surface area, where the adsorbed water can account for several weight percent of the total sample mass, makes it possible to effectively apply neutron scattering (normally, a bulk-sensitive technique) for studying the surface water dynamics [3–10], due to the exceptionally high incoherent neutron scattering cross section of hydrogen. An important advantage of neutron scattering [in particular, quasielastic neutron scattering (QENS)] is that the dependence of the scattering signal on the momentum transfer Q can yield valuable information about the spatial characteristics of the diffusion processes. The new generation of QENS-capable neutron spectrometers has a great potential for detailed studies of various diffusion components in surface water, due to their high neutron flux and high ratio of the accessible energy transfer to the energy resolution (the dynamic range). Previously, we successfully probed the dynamics of surface water in nanopowder rutile, TiO_2 [9], using a backscattering spectrometer, BASIS [12], which was then undergoing commissioning, at the Spallation Neutron Source (SNS) at Oak Ridge National Laboratory (ORNL), USA. Together with molecular dynamic (MD) simulation, the compilation of the data collected at the BASIS and in the previous QENS studies of water on rutile revealed the presence of at least three dynamic components in the hydration water on the pico- to nanosecond time scale. The slowest dynamic component was attributed to the translationlike motions (e.g., interlayer jumps between L_2 and L_3) that involve rearrangement of the cage made by the neighboring water molecules. Qualitatively, these slowest motions are similar to (but much slower than) translational diffusion jumps in bulk water, except that in surface water these motions are spatially confined. The intermediate dynamic component was ascribed to localized, rotationlike motions of the water molecules in all layers, rather similar in character to (albeit significantly slower than) rotational diffusion jumps in bulk water. Finally, the fastest dynamic component was related predominantly to the diffusion dynamics of the outermost layer, L_3, where the water molecules exhibit, on average, significantly fewer hydrogen bonds than bulk water. This leads to a diffusion component with no analog in bulk water. Interestingly, in the earlier studies, this fast component could not be resolved at all below 250 K, which prompted questions regarding possible "surface freezing" in hydration water on cooling down (which would be the opposite of "surface melting" on warming up).

At the time of that study, the still low SNS power and relatively high backgrounds precluded analysis of the Q dependence of the data. In this work, we have revisited the dynamics of hydration water in nanopowder rutile, using the much improved BASIS (and the SNS at the much increased power level) together with another recently commissioned SNS spectrometer, a direct geometry time-of-flight Cold Neutron Chopper Spectrometer (CNCS). The data collected at the BASIS and CNCS are revealing a complex picture of the temperature dependence of the diffusion processes in surface water. As we discuss in this paper, all of the

*mamontove@ornl.gov

previously discovered diffusion components, including the fastest component due to the dynamics of underbonded water molecules, are present in the temperature range of at least 230–320 K. While the dynamics of all components slow down at lower temperatures, the experiment provides, at first sight, no evidence of a discontinuity in the dynamics of hydration water within the temperature range studied. However, a qualitative change in the elastic scattering between 240 and 250 K suggests an effective surface freezing-melting transition, when the motions that are localized at lower temperatures become delocalized between 240 and 250 K. Only at 250 K and above can the motions of the hydration water molecules on the nanosecond time scale be viewed as spatially unrestricted.

II. EXPERIMENT

Two neutron scattering spectrometers at the SNS were used in this study. One is the near-backscattering spectrometer BASIS [12], and the other is the Cold Neutron Chopper Spectrometer (CNCS). For the chosen experimental setup, the BASIS had an energy resolution of 3.4 μeV (full width at half maximum, for the Q-averaged resolution value) and a useful dynamic range of ± 100 μeV. The CNCS was operated with an incident wavelength of 7.3 Å in "high-intensity" mode, resulting in a Q-averaged energy resolution of 24 μeV (full width at half maximum) and a dynamic range suitable for the QENS data analysis of ± 1.0 meV.

The rutile nanopowder was prepared, characterized, and hydrated following the procedures described in great detail in a previous paper [8]. The TiO_2 nanocrystals have a rodlike or truncated-rodlike habit and have an average length of $\sim$10 nm with aspect ratios from 1:1 to 1:6. The specific surface area of the nanoparticles was determined using the N_2 Brunauer-Emmett-Teller (BET) method, yielding 181.3 $m^2/g \pm 0.3$ m^2/g (theoretical bulk density 4.25 g/cm^3). Hydration of the dry TiO_2 nanopowders was carried out by allowing the powders to equilibrate with laboratory air ($\sim$23 °C and 80% relative humidity) for a period of $\sim$24 h prior to loading in aluminum sample cans [8]. Thus the TiO_2 sample appears to have $\sim$3.5 H_2O molecules per Me_2O_4 surface unit [8]. The QENS data used in the presented analysis were collected on warming up, at seven different temperatures $T = 230$, 240, 250 260, 280, 300, and 320 K at both BASIS and CNCS. In addition, prior to the temperature-dependent measurements, two sets of data were collected at 4 and 5 K on BASIS and CNCS, respectively, and were used to characterize the energy resolution of the instruments. Flat-plate sample holders (at 135 ° with respect to the incident beam) were used, with the sample thickness (0.5 mm) carefully controlled to ensure $\sim$95% transmission of the incident beam through the sample in order to minimize the effects of multiple scattering, which is especially important for the data collected at low scattering angles (that is, at low Q values).

III. RESULTS AND DISCUSSION

While diffusion dynamics of water in the bulk form can be successfully described by either two Debye-like processes [13] or the relaxing cage model (RCM) [14,15], the dynamics of surface water measured over the pico- to nanosecond range requires a more complex description. This is likely because of the effects that the surface exerts on the hydrated water, which, because of the small thickness of the hydration layers (<8 Å) [9], are more prominent than for water in a typical nanoconfinement configuration. Besides, the presence of the outermost hydration layer, with its underbonded water molecules, is what further differentiates surface water from nanoconfined water. While each of the several components describing the diffusion dynamic of surface water is, to a different extent, of non-Debye character, data fits that involve more than one independent stretched exponential term would not be robust. Thus, we rely on the previously described fit procedure [9] which, while assuming a simplified, Debye-like time dependence of each component, properly distinguishes between the translationlike and rotationlike motions and the even faster component, in accordance with the MD results [9]. The QENS data were fit using the expression [9]

$$I(E) = [x\delta(E) + (1-x)S(E) + B(E)] \otimes R(E). \quad (1)$$

Here x represents the fraction of the elastic scattering, $\delta(E)$ is a delta function centered at zero energy transfer, $B(E)$ is the linear background term in the form of $B(E) = C_1 + C_2 E$, $R(E)$ is the resolution function, and $S(E)$ is the model scattering function. As we will explain below, we attempted to fit all the data sets collected on the CNCS using three Lorentzian components (3L model):

$$S(Q,E) = p_b(Q)\frac{1}{\pi}\frac{\Gamma_1(Q)}{E^2+\Gamma_1^2(Q)} + p_i(Q)\frac{1}{\pi}\frac{\Gamma_2(Q)}{E^2+\Gamma_2^2(Q)} + p_n(Q)\frac{1}{\pi}\frac{\Gamma_3(Q)}{E^2+\Gamma_3^2(Q)}. \quad (2)$$

This functional form includes a broad, an intermediate, and a narrow component. The broad and intermediate components have spectral weights of $p_b(Q)$ and $p_i(Q)$, while the narrow component has a spectral weight of $p_n(Q) = 1 - p_b(Q) - p_i(Q)$. For the data sets obtained from BASIS, since the dynamic range is narrower, the broadest Lorentzian component that was evident in the CNCS data could not be detected reliably. Thus, we use the two-Lorentzian model (2L model) and $p_b(Q)$ in Eq. (2) is set to 0 in the fitting. The $S(E)$ now can be written in the form

$$S(Q,E) = p_n(Q)\frac{1}{\pi}\frac{\Gamma_1(Q)}{E^2+\Gamma_1^2(Q)} + p_i(Q)\frac{1}{\pi}\frac{\Gamma_2(Q)}{E^2+\Gamma_2^2(Q)}, \quad (3)$$

where $p_n(Q)$ indicates the spectral weight of the narrower of the two components and $p_i(Q) = 1 - p_n(Q)$ is the spectral weight of the broader of the two components. Furthermore, at low temperatures (in this study, below 250 K) for the data obtained on the CNCS, the narrowest component becomes too narrow to detect, i.e., falls within the range of the spectrometer resolution. In this case, the 3L model turns into the 2L model. As we will discuss later, both the broader component of the BASIS fits and the intermediate component of the CNCS fits likely describe the same dynamic component of the hydration water. Thus we refer to the broader of the two BASIS fit components as intermediate.

The reasons why, in this study, we concentrated on the temperature region between 230 and 320 K are as follows. The slowest of the studied components (on the nanosecond

time scale) is known to exhibit a dynamic crossover below 230 K, where its temperature dependence measured by QENS undergoes a profound change [16–21]. Recently, there have been suggestions [22] that this dynamic crossover might be an inherent property of supercooled water which is related to the split of a secondary relaxation component from the main component. In such a scenario, the actual number of distinct dynamic components in surface water increases below the dynamic crossover. As this question is not yet resolved, we wanted to limit our analysis to temperatures above the dynamic crossover, where the number of the dynamic components is not disputed. In our opinion, the energy resolution of the BASIS, while sufficient to merely detect the presence of the dynamic crossover in the data, would not be adequate to distinguish between the scenarios that involve different numbers of dynamic components below the crossover temperature. As for the high limit of our temperature range, the CNCS data revealed some desorption of the surface water above 320 K. Therefore, the analysis was limited to the temperature range where the amount of the hydration water on the rutile surface remained unchanged.

Figures 1 and 2 show the temperature dependence of the raw data and the fitting procedure, respectively. We analyzed the data at six Q values, ranging from 0.5 to 1.5 Å^{-1}, in 0.2-Å^{-1} steps. The temperature dependence of the relaxation times obtained from both the BASIS and CNCS data is shown

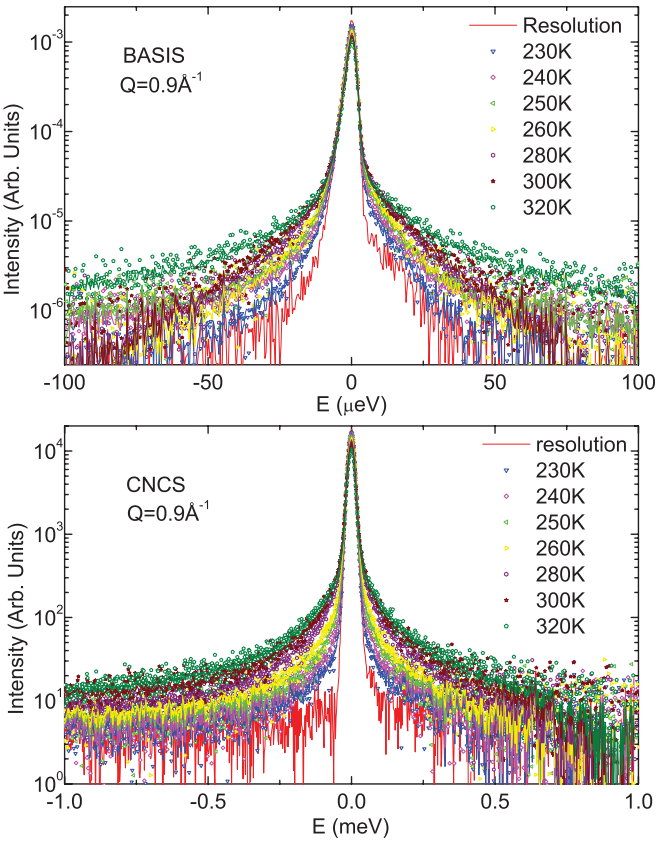

FIG. 1. (Color online) Scattering intensities collected on BASIS and CNCS at $Q = 0.9$ Å^{-1}, at seven different temperatures $T = 320$, 300, 280, 260, 250, 240, and 230 K. The innermost red lines are resolution functions for each instrument. The solid lines are the fits using Eqs. (1)–(3).

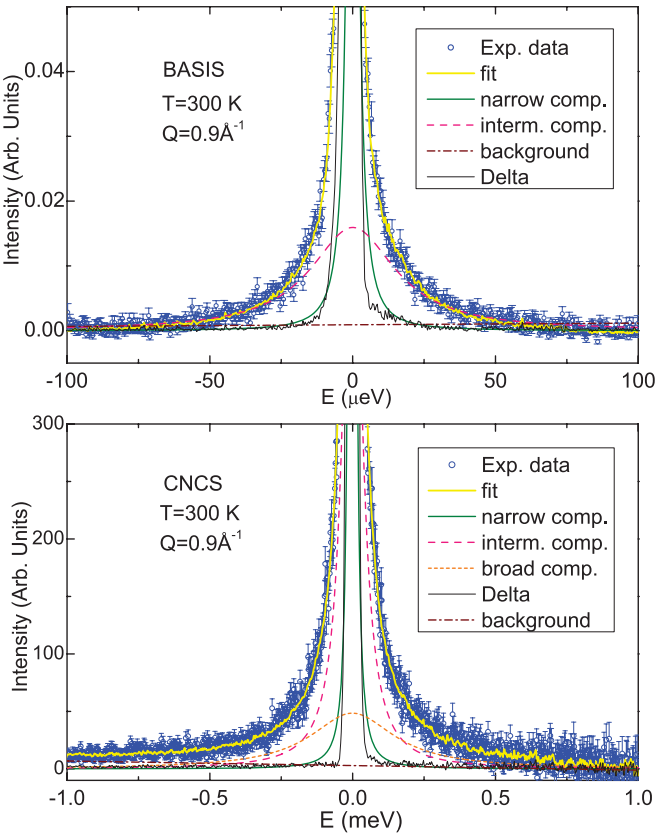

FIG. 2. (Color online) Analysis of the QENS spectra taken from BASIS and CNCS according to Eqs. (1)–(3). Circles indicate the experimental data and the yellow solid lines the 2L and 3L model fits. The orange dotted line, pink dashed lines, and the green solid lines are the broad, intermediate, and narrow components of the models convolved with energy resolution function of the instrument, respectively. We show results at $Q = 0.9$ Å^{-1} and $T = 300$ K.

in Fig. 3. The relaxation times τ are calculated from the Lorentzian half width at half maximum, Γ, as $\tau = \hbar/\Gamma$. Importantly, the relaxation times presented in Fig. 3 are model independent, in a sense that they were obtained separately at each Q value, using no assumption about their Q dependence and the character of the relaxation processes (translational, rotational, etc.). Thus, each graph in Fig. 3 represents the relaxation times that are associated with the diffusion dynamics apparent on a particular length scale (inversely proportional to the Q value) and measured separately by the two different spectrometers.

It is obvious that both spectrometers probe the same three dynamic components in the hydration water (except for the fastest, i.e., broadest, component, which is beyond the BASIS dynamic range). The relationship between the actual three dynamic components, as found in the earlier MD analysis [9] (fast, intermediate, and slow), and the fit components (broad, intermediate, and narrow) can be summarized as follows:

(a) The fast dynamic component: cannot be seen on the BASIS, detected as the broad component in the CNCS fits (orange spheres in Fig. 3).

(b) The intermediate dynamic component: detected as the intermediate components in the BASIS fits (yellow triangles in Fig. 3) and the CNCS fits (pink diamonds in Fig. 3).

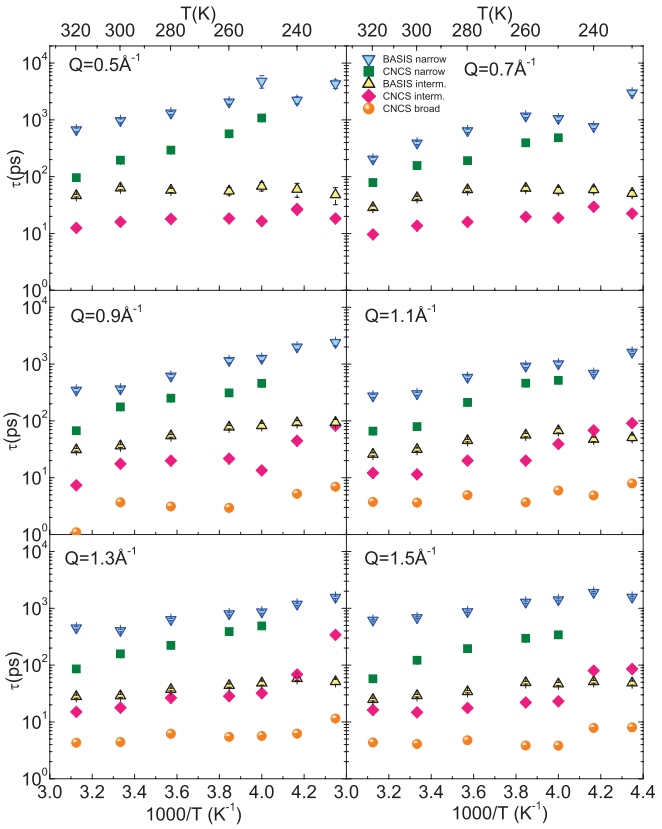

FIG. 3. (Color online) The relaxation times calculated from QENS spectra taken from BASIS and CNCS at six different Q values, $Q = 0.5$, 0.7, 0.9, 1.1, 1.3, and 1.5 Å^{-1}, as a function of temperature.

(c) The slow dynamic component: detected as the narrow component in the BASIS fits (blue triangles in Fig. 3) and the narrow component in the CNCS fits (green squares in Fig. 3).

The agreement between the BASIS and CNCS fit components is better for the intermediate dynamic component. This is because the intermediate dynamic component is on the time scale of tens of picoseconds, which falls comfortably in the dynamic range of both spectrometers. For this component, the relaxation times obtained from the BASIS data are only somewhat longer compared to those obtained from the CNCS. The slowest dynamic component is close to the resolution limit of the CNCS and is better captured by the BASIS; hence, one can see greater disagreement between the two spectrometers for the narrow fit components, where the BASIS relaxation times are systematically longer. It has been demonstrated by Magazu *et al.* [23] that the apparent relaxation times obtained on a particular spectrometer are largely defined by its energy resolution once they become long enough to exceed the resolution limit of the spectrometer. In fact, at the lowest two temperatures (240 and 230 K), the slow dynamic component becomes too narrow for the CNCS to detect, as one can see in Fig. 3, where the 2L model needs to be used instead of the 3L model for the CNCS data. Our choice of the 2L model over the 3L model for the CNSC data fits below 250 K is not arbitrary, as one can see from Table I. For the temperatures above 240 K, fits using the 3L model show a better agreement factor compared to the 2L model. This indicates that the CNCS can detect all three dynamic components (fast, intermediate, and slow) above 240 K. However, at 240 K and below, 2L fits show better agreement compared to the 3L fits, indicating that at low temperatures, the slow dynamic component yields too narrow a QENS signal to be detected by CNCS. The disappearance of the narrow component from the CNCS fits does not indicate the actual disappearance of the slow dynamic component, as this slow dynamic component is obviously present in the BASIS low-temperature data.

At the low Q values of 0.5 and 0.7 Å, the CNCS data fits again exhibit two instead of three fit components, regardless of the temperature. The disappearance of the broad fit component from the CNCS data at low Q cannot be related to limitation due to either the resolution or the dynamic range of the spectrometer. Indeed, even if the QENS broadening were Q dependent, indicating a translational diffusion process, it could only decrease, but not increase, at the lower Q values. That is, the measured relaxation times could be only longer, but not shorter at low Q compared to the higher Q, which would bring the broad component comfortably into the dynamic range of the CNCS. Instead, the disappearance of the broad component at low Q must be indicative of spatial localization of the dynamics that yield this broad component. However, it is not plausible that the dynamics associated with the underbonded water molecules, predominantly of the outermost hydration layer, could be more spatially localized compared to the rotational (that is, "inside the cage") dynamics of all hydration water molecules. The latter dynamics are certainly more spatially localized, and, thus, should disappear more quickly in the low-Q data. Therefore, even though we chose to show the fast, not the intermediate CNCS fit component disappear at low Q in the model-independent color scheme presentations of the relaxation times in Fig. 3, one needs to realize that it is likely the fast, not the intermediate dynamic component that manifests itself in the set of the shorter CNCS relaxation times

TABLE I. Comparison of fitting residuals of the CNCS data using two different model functions: two Lorentzians (2L) and three Lorentzians (3L) at four different Q values and six temperatures.

	$Q = 0.9$ Å^{-1}		$Q = 1.1$ Å^{-1}		$Q = 1.3$ Å^{-1}		$Q = 1.5$ Å^{-1}	
	2L	3L	2L	3L	2L	3L	2L	3L
320 K	0.903	0.877	1.361	1.210	1.874	1.770	1.733	1.606
300 K	0.955	0.907	1.168	1.107	1.789	1.688	1.806	1.578
280 K	0.939	0.897	1.060	1.016	1.392	1.343	1.466	1.368
260 K	0.928	0.906	1.049	1.013	1.212	1.150	1.226	1.135
250 K	0.956	0.946	1.152	1.131	1.195	1.155	1.237	1.163
240 K	1.070	1.073	1.001	1.005	1.041	1.044	0.994	1.024

at $Q = 0.5$ and 0.7 Å^{-1}, while the intermediate component disappears. Because of the long-range, translational character of the fast dynamic component, the relaxation times associated with it grow longer at low Q to become comparable with the intermediate dynamic component relaxation times. Yet it is the fast, not the intermediate dynamic component that manifests itself in the low-Q data, where the intermediate component does not contribute to the QENS broadening because of its spatial localization. In other words, the more localized, true rotational component represents the intermediate motions at higher Q values and practically disappears at low Q values. At the same time, the fast motions, which are of partially translational character, yield the Q-dependent broadening that narrows down at low Q value and can be easily mistaken for the intermediate motions, even though the latter should not actually contribute to the QENS signal at low Q.

Figures 4 and 5 show the temperature and Q dependence, respectively, of the total elastic scattering fraction [parameter x in Eq. (1)] and the spectral weights of the quasielastic fit components [parameters p_b, p_i, and p_n in Eqs. (2) and (3)]. The color scheme used for these figures is the same as used for Fig. 3. Thus, the same components, which cannot be found in the fits at some temperature and Q points, are missing in Figs. 3–5. In most cases, there is a reasonable agreement between the spectral weights of the narrow CNCS and narrow BASIS components. The same applies to the spectral weights of the intermediate CNCS and intermediate BASIS components. These observations confirm our conjecture that each of these two pairs of components describes the same dynamics, even though the agreement between the p parameters from the CNCS and BASIS fits may be less than perfect, depending on the interplay between the resolution and dynamics range of the measurements. The fast CNCS component has no counterpart in the BASIS fits, due to a limited dynamic range of the latter. There is also at least a qualitative agreement in the elastic scattering fractions between the CNCS and BASIS fits. One important observation that comes from Fig. 4 is that the elastic scattering in the CNCS data increases very significantly below 250 K, even though this increase is much less pronounced in the BASIS data. This increase is related to the behavior of the broad CNCS component that originates from the fastest dynamics in the system, inaccessible in the BASIS experiment. At 240 and 230 K, the elastic scattering fraction in the CNCS data approaches unity in the limit of low Q, as one can readily see from the Q dependence presented in Fig. 5. This is a well known sign of a spatially restricted diffusion process. As we have mentioned above, in the earlier Q-independent studies [9] the broad component could not be resolved at all below 250 K, whereas in the current experiment it can be detected. It appears that some discontinuity in the dynamics of the hydration water indeed takes place between 240 and 250 K. The fast motions in the hydration water that were present even at lower

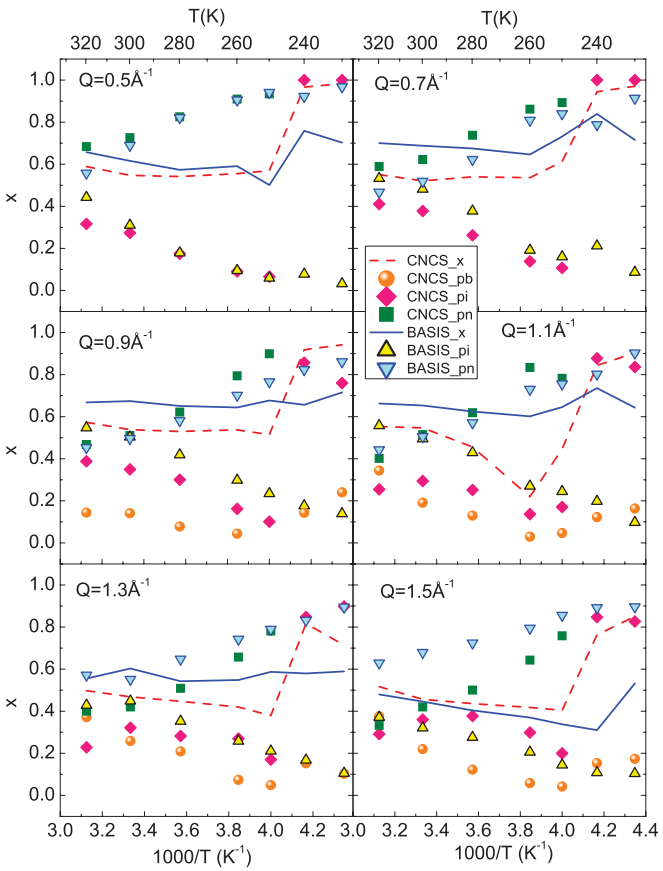

FIG. 4. (Color online) The elastic scattering fractions [parameter x in Eq. (1), lines] and spectral weights of the quasielastic fit components [parameters p_b, p_i, and p_n in Eqs. (2) and (3), symbols] as a function of temperature.

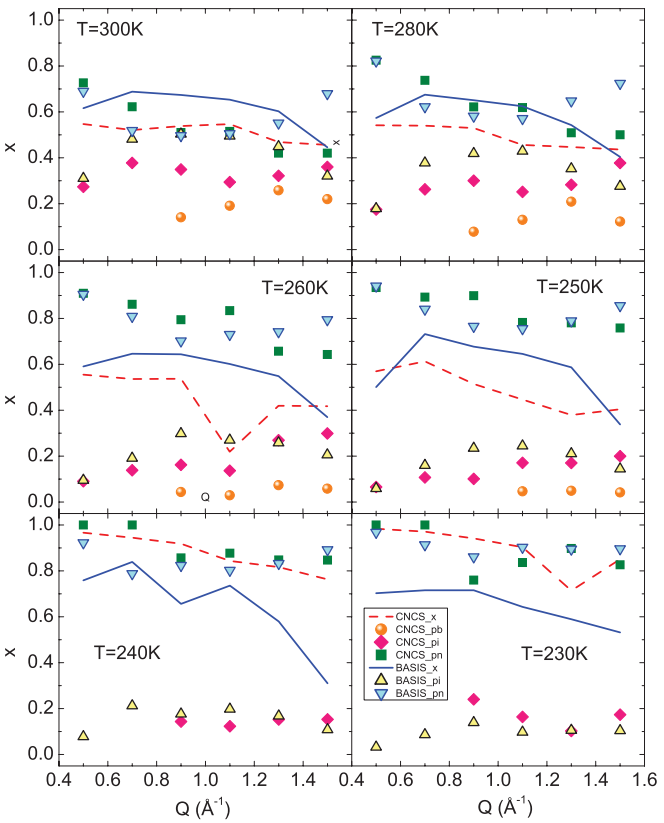

FIG. 5. (Color online) The elastic scattering fractions [parameter x in Eq. (1), lines] and spectral weights of the quasielastic fit components [parameters p_b, p_i, and p_n in Eqs. (2) and (3), symbols] as a function of Q.

temperatures but had a spatially restricted character assume a character of spatially unrestricted translational diffusion between 240 and 250 K. This is a discontinuity that resembles the "surface melting" observed in multilayered ice on MgO surfaces [24].

As we have mentioned above, the energy resolution of the BASIS may not be sufficient to distinguish between different scenarios of the dynamical behavior of hydration water at low temperatures. Experiments with higher resolution, such as neutron spin echo, may be required. Alternatively, broadband dielectric spectroscopy can be effectively applied to study dynamics of hydration water on a time scale spanning many orders of magnitude. While lacking the Q-resolution capabilities of neutron scattering techniques, dielectric spectroscopy does not suffer from energy resolution limitations of the former, which, in studies of hydration water, allows one to venture into the low-temperature region. In particular, a very recent study of protein hydration water that combined broadband dielectric spectroscopy and Monte Carlo simulations indicated the presence of two dynamic crossovers, at ∼181 and 252 K (but not at any temperature in between) [25]. The location of the lower-temperature crossover, attributed to the cooperative reordering of the hydrogen bond network, seems to be in agreement with the earlier dielectric spectroscopy study of hydration water [26]. The higher-temperature crossover is attributed to a change in the diffusion regime of water protons, from subdiffusive at lower temperatures to freely diffusive at higher temperatures [27]. Even though the relaxation times at which this crossover is observed in dielectric measurements are much longer compared to the time scale of our neutron measurement, there is a remarkable similarity between these two experiments in both the measured temperature of the crossover and its interpretation as a transition to the diffusive regime above the crossover temperature.

In essence, the present study suggests that in the entire temperature range of 230–320 K, there exist the dynamic components previously assigned to interlayer (L_2-L_3) jumps, rotational jumps in all layers, and the dynamics of the outermost layer. However, it is only between 240 and 250 K when the unrestricted translationlike diffusion develops. At lower temperature, all the dynamic processes present in the system are of localized character.

To this point, our discussion concerned only the model-independent relaxation times directly extracted from the data fits. Now we plot the data (see Fig. 6) using the more commonly utilized representation to show the Q dependence of the QENS broadening at each measured temperature. The new color scheme adopted in Fig. 6 is model dependent, in a sense that, unlike for the scheme used in Figs. 3–5, we now use some assumptions about associations of each measured relaxation time with a particular diffusion component. The color scheme in Fig. 6 is adopted primarily to illustrate the difficulties that one may encounter using the traditional approach of the analysis of the Q dependence of the QENS data from hydration water. Each dynamic component, slow, intermediate, and fast, manifests itself in the QENS broadening that is always somewhat wider on the CNCS compared to the BASIS, in agreement with the narrower dynamics range and better energy resolution of the latter. The graphs for 240 and 230 K differ from the rest of the graphs in only one respect: The slow component, which yields a very narrow signal at these temperatures, cannot be resolved in the CNCS data.

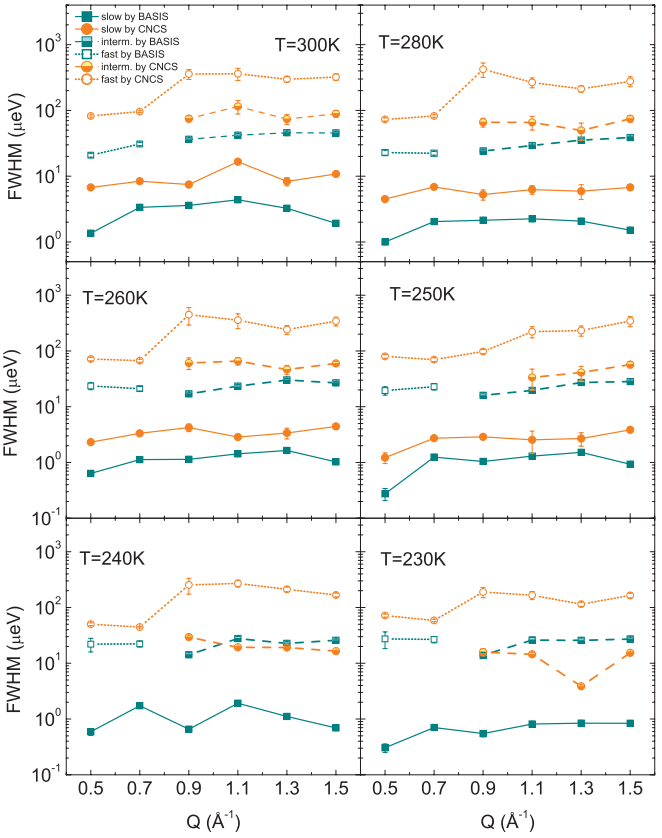

FIG. 6. (Color online) Dynamic processes represented by different groups of Lorentzian full width at half maximum (FWHM) at six different temperatures $T = 300$, 280, 260, 250, 240, and 230 K. The solid, dashed, and dotted lines are a "guide for the eye," indicating the fast, intermediate, and slow dynamic components probed by the BASIS and CNCS.

The more interesting observation concerns the relaxation times obtained at $Q = 0.5$ and 0.7 Å^{-1} (irrespective of the temperature). Given the more spatially localized character of the rotational diffusion (the intermediate component), which should lead to disappearance of the corresponding QENS broadening at low Q, we contend that the intermediate component in the BASIS data fits at $Q = 0.5$ and 0.7 Å^{-1} actually represents not the intermediate dynamic component (as it does at the higher Q values), but the fast dynamic component instead. This consideration suggests that in QENS studies of hydration water, in general, neutron backscattering spectrometers, which are characterized by the high energy resolution and a limited dynamic range, probe different dynamic components, depending on the Q value of the measurement. The narrower QENS signals in the backscattering measurements always represent the slow dynamic component, associated with the translationlike motions, such as L_2-L_3 interlayer jumps. Although translational in character, in a sense that they involve motions of the molecule center of mass and multiple hydrogen bond breaking, these motions are spatially localized, thus yielding a Q-independent QENS signal.

The broader QENS signals in the backscattering measurements at low Q represent the fast dynamic component, which is

primarily associated with the outermost hydration layer. This component is of translational character, and, as such, broadens with increasing Q. At higher Q values, it grows beyond the dynamic range of the backscattering measurement, which then instead begins to probe a different, rotational dynamic component, which is not present in the low-Q data because of its spatially localized character. This rotational component is slower compared to the dynamics of the outermost water molecules, and is often within the dynamic range of the backscattering measurements. This consideration suggests that attempts to fit the Q dependence of the broader QENS signals from hydration water may often lead to wrong conclusions. For example, the diffusion coefficient determined from the low-Q data, and the relaxation times determined from the high-Q data may actually be related to different dynamic components; the dynamics of the underbonded water molecules and the rotational dynamics, respectively. Prior knowledge of the spatial characteristics of each dynamic component, based on the results of MD simulations [8–10], is thus essential for the correct assignment of the dynamic components to each fit component in the QENS data.

IV. CONCLUSION

We attempted a model-independent analysis of the QENS data from the hydration water on rutile collected on two neutron spectrometers with different dynamic ranges and energy resolutions, a backscattering and a disk chopper time-of-flight. We resolved three dynamic components, each associated with particular diffusion motions. All three dynamic components were present through the entire studied temperature range of 230–320 K. A qualitative change in the elastic scattering between 240 and 250 K suggests an effective surface freezing-melting transition, when the motions that are localized at lower temperatures become delocalized between 240 and 250 K. Only at 250 K and above can the motions of the hydration water molecules on the nanosecond time scale be viewed as spatially unrestricted. Our analysis suggests that, in general, a QENS experiment on such a complex system as hydration water may probe different dynamic components, depending on the analyzed Q value. Thus, prior knowledge of the spatial characteristics of each dynamic process, most likely from MD simulations, is essential to correctly assign each measured QENS broadening component to a particular type of diffusion motion.

ACKNOWLEDGMENTS

This work was sponsored by the Division of Chemical Sciences, Geosciences, and Biosciences, Office of Basic Energy Sciences, US Department of Energy. The neutron scattering experiment at Oak Ridge National Laboratory's Spallation Neutron Source was sponsored by the Scientific User Facilities Division, Office of Basic Energy Sciences, US Department of Energy.

[1] C. H. Sun, L. M. Liu, A. Selloni, G. Q. Lu, and S. C. Smith, J. Mater. Chem. **20**, 10319 (2010).
[2] M. Predota, P. T. Cummings, and D. J. Wesolowski, J. Phys. Chem. C **111**, 3071 (2007).
[3] Y. Kuroda, S. Kittaka, S. Takahara, T. Yamaguchi, and M. C. Bellissent-Funel, J. Phys. Chem. B **103**, 11064 (1999).
[4] S. Takahara, S. Kittaka, T. Mori, Y. Kuroda, T. Yamaguchi, and K. Shibata, J. Phys. Chem. B **106**, 5689 (2002).
[5] E. Mamontov, J. Chem. Phys. **121**, 9087 (2004).
[6] E. Mamontov, J. Chem. Phys. **123**, 024706 (2005).
[7] E. Mamontov, J. Chem. Phys. **123**, 171101 (2005).
[8] E. Mamontov, L. Vlcek, D. J. Wesolowski, P. T. Cummings, W. Wang, L. M. Anovitz, J. Rosenqvist, C. M. Brown, and V. G. Sakai, J. Phys. Chem. C **111**, 4328 (2007).
[9] E. Mamontov, D. J. Wesolowski, L. Vlcek, P. T. Cummings, J. Rosenqvist, W. Wang, and D. R. Cole, J. Phys. Chem. C **112**, 12334 (2008).
[10] E. Mamontov, L. Vlcek, D. J. Wesolowski, P. T. Cummings, J. Rosenqvist, W. Wang, D. R. Cole, L. M. Anovitz, and G. Gasparovic, Phys. Rev. E **79**, 051504 (2009).
[11] N. Kumar, S. Neogi, P. R. C. Kent, A. V. Bandura, J. D. Kubicki, D. J. Wesolowski, D. Cole, and J. O. Sofo, J. Phys. Chem. C **113**, 13732 (2009).
[12] E. Mamontov and K. W. Herwig, Rev. Sci. Inst. **82**, 085109 (2011).
[13] J. Teixeira, M.-C. Bellissent-Funel, S. H. Chen, and A. J. Dianoux, Phys. Rev. A **31**, 1913 (1985).
[14] S. H. Chen, C. Liao, F. Sciortino, P. Gallo, and P. Tartaglia, Phys. Rev. E **59**, 6708 (1999).
[15] C. Y. Liao, F. Sciortino, and S. H. Chen, Phys. Rev. E **60**, 6776 (1999).
[16] A. Faraone, L. Liu, C. Y. Mou, C. W. Yen, and S. H. Chen, J. Chem. Phys. **121**, 10843 (2004).
[17] L. Liu, S. H. Chen, A. Faraone, C. W. Yen, and C. Y. Mou, Phys. Rev. Lett. **95**, 117802 (2005).
[18] S. H. Chen, L. Liu, X. Chu, Y. Zhang, E. Fratini, P. Baglioni, A. Faraone, and E. Mamontov, J. Chem. Phys. **125**, 171103 (2006).
[19] S. H. Chen, L. Liu, E. Fratini, P. Baglioni, A. Faraone, and E. Mamontov, Proc. Natl. Acad. Sci. USA **103**, 9012 (2006).
[20] X. Q. Chu, E. Fratini, P. Baglioni, A. Faraone, and S. H. Chen, Phys. Rev. E **77**, 011908 (2008).
[21] Y. Zhang, M. Lagi, F. Ridi, E. Fratini, P. Baglioni, E. Mamontov, and S. H. Chen, J. Phys.: Condens. Matter **20**, 502101 (2008).
[22] E. Mamontov, A. Faraone, E. W. Hagaman, K. S. Han, and E. Fratini, J. Phys. Chem. B **114**, 16737 (2010).
[23] S. Magazu, F. Migliardo, and A. Benedetto, J. Phys. Chem. B **115**, 7736 (2011).
[24] C. Toubin, S. Picaud, P. N. M. Hoang, C. Girardet, B. Demirdjian, D. Ferry, and J. Suzanne, J. Chem. Phys. **114**, 6371 (2001).
[25] M. G. Mazza, K. Stokely, S. E. Pagnotta, F. Bruni, H. E. Stanley, and G. Franzese, eprint arXiv:0907.1810v2 (2011).
[26] J. Swenson, H. Jansson, J. Hedstrom, and R. Bergman, J. Phys.: Condens. Matter **19**, 205109 (2007).
[27] S. E. Pagnotta, R. Gargana, F. Bruni, and A. Bocedi, Phys. Rev. E **71**, 031506 (2005).